Atmos. Meas. Tech., 17, 1037–1050, 2024
https://doi.org/10.5194/amt-17-1037-2024

Atmospheric Measurement Techniques
Open Access
EGU

Development and characterization of a high-performance single-particle aerosol mass spectrometer (HP-SPAMS)

Xubing Du[1,3], Qinhui Xie[1,3], Qing Huang[1,3], Xuan Li[1,3], Junlin Yang[2], Zhihui Hou[2], Jingjing Wang[2], Xue Li[1,3], Zhen Zhou[1,3], Zhengxu Huang[1,3], Wei Gao[1,3], and Lei Li[1,3]

[1]Institute of Mass Spectrometer and Atmospheric Environment, Jinan University, Guangzhou, 510632, China
[2]Guangzhou Hexin Analytical Instrument Limited Company, Guangzhou, 510530, China
[3]Guangdong Provincial Engineering Research Center for on-line source apportionment system of air pollution, Guangzhou, 510632, China

Correspondence: Lei Li (lileishdx@163.com)

Received: 2 September 2022 – Discussion started: 1 November 2022
Revised: 19 August 2023 – Accepted: 9 December 2023 – Published: 13 February 2024

Abstract. This study describes a high-performance single-particle mass spectrometry (HP-SPAMS) design in detail. The comprehensive improvements in the injection system, optical sizing system, mass spectrometry, and data acquisition system have improved particle detection efficiency and chemical analysis. The combination of an aerodynamic particle concentrator (APC) system and a wide range of aerodynamic lenses (ADLs) enables the concentration of particles in the 100–5000 nm range. Using an APC increases the instrument inlet flow by a factor of 3–5. The ion delayed-exaction technology of bipolar time-of-flight mass spectrometry improves the mass resolution by 2–3 times, allowing the differentiation of isobaric ions of different substances. Moreover, the four-channel data acquisition technology greatly enhances the dynamic range of mass spectrometry. The improved HP-SPAMS enhances the overall capability of the instrument in terms of particle detection number and scattering efficiency. Moreover, it improves accuracy and sensitivity for component identification of individual particles.

The experimental performance of HP-SPAMS shows that the scattering efficiency of polystyrene latex microspheres is almost 70 %–100 % in the range of 300–3000 nm. Compared to the previous SPAMS, HP-SPAMS has a larger inlet flow rate and scattering efficiency and a higher laser frequency, which makes HP-SPAMS increase the effective number of particles detected and improve the temporal resolution of detection. For the analysis of individual particles, HP-SPAMS achieves an average mass spectral resolution of 2500 at m/z 208, which helps distinguish between most organic fragment ions and metal ions and facilitates the analysis of complex aerosol particles. For the analysis of individual particles, the increased resolution of the HP-SPAMS contributes to the differentiation of most organic fragment ions and metal ions and facilitates the evaluation of complex aerosol particles, in the case of atmospheric lead-containing particles. The improved detection efficiency and chemical analysis capability of HP-SPAMS will be of great importance for low-concentration aerosol detection and complex aerosol component analysis.

1 Introduction

Atmospheric aerosols impact atmospheric visibility, cloud formation, and rainfall, among others, and have been the focus of research on atmospheric physicochemical processes (McNeill, 2017; Pöschl, 2005). Single-particle aerosol mass spectrometry (SPMS; e.g., Murphy, 2007) can analyze information such as particle size and composition at the level of individual aerosols in real time. Moreover, it has the advantage of a fast response time and high sensitivity, which has been applied to investigate environmental climate and atmospheric chemistry (Murphy et al., 2006; Zhang et al., 2015, 2009). However, due to the limitations of the SPMS detection capabilities, simultaneous detection with high temporal and spatial resolutions in low-concentration environments is not yet well realized. One reason is that the low inlet flow rates and poor transport efficiencies limit the number of aerosols

that SPMS can analyze in low-concentration environments, such as high-altitude mountainous or the atmospheric stratosphere (Jost et al., 2004; Schmidt et al., 2017). Although enough particles can be obtained by long-time collection, this would result in a loss of temporal or spatial resolution, especially on airborne or shipboard instruments (Sun et al., 2019). Thus, improving the collection capability of SPMS is necessary for accurate analysis. Another reason is the low mass resolution and detection sensitivity of SPMS, leading to possible problems with the capability in terms of aerosol characterization; e.g., Liu et al. (2017) found in their study that vanadium markers (V^+ or VO^+) emitted from ships were interfered with isobaric organic ions.

The number of particles detected in real time is closely related to the inlet flow rate, the particle transmitting efficiency, and the particle detection efficiency (Li et al., 2011; Murphy, 2007; Noble and Prather, 2000; Pratt and Prather, 2012). The commonly used aerodynamic lens inlet systems have good particle focusing performance, but the transmitted flow rate limits the inlet flow rate (Liu et al., 1995; Wang et al., 2005). Increasing the inlet flow rate could increase the number of particles detected per unit time in SPMS. Cahill et al. (2014) developed a high-flow-rate injection system by combining a virtual impactor with an aerodynamic lens. Our team also developed a particle concentration device to increase the injection flow rate by a factor of 5 (Zhuo et al., 2021). The transmission efficiency of the inlet system also affects the number of particles measured since some particles are lost in the critical orifice, buffer chamber, etc. (Chen et al., 2007; Hwang et al., 2015). At the same time, the small divergence of the aerodynamic lens can lead to a large transmission divergence of particles over long distances, which are difficult to detect by means of the sizing–ionization optical system, especially for non-spherical particles (Clemen et al., 2020; Murphy, 2007; Zelenyuk et al., 2009). The particles transmitted to the instrument through the inlet system are not fully measurable, which could also be related to the particle-sizing efficiency and ionization probability (Gemayel et al., 2016).

The sizing efficiency could be improved by increasing the intensity of the collected scattered light signal (Zawadowicz et al., 2020) or by optimizing the optical path and selecting a more sensitive detector to improve the signal-to-noise ratio (Zelenyuk et al., 2009). Whether the particles could be ionized or not is not only connected to the particle focusing characteristics of the inlet system and the accuracy of the measurement of the sizing system but is also related to the particle composition, the maximum operating frequency, wavelength, the energy threshold of the ionization laser, etc. (Thomson et al., 1997; Zelenyuk et al., 2008).

The detection sensitivity and mass spectral resolution of SPMS directly affects its ability to analyze individual complex-component aerosols. The sensitivity of single-particle detection is mainly related to the ion yield of the laser ionization of the particles (Zawadowicz et al., 2015). Previous studies have shown that the ion yield and ablation depth of the laser depend on the laser energy density (Cahill et al., 2015; Wenzel and Prather, 2004), with low energy resulting in a low threshold to be dissociated and high energy increasing the abundance of organic fragmentation (Thomson et al., 1997). Therefore, the non-uniform Gaussian beam usually used in SPMS could make the particles fall at different locations and obtain different energies, resulting in different sensitivity responses by different particles (Steele et al., 2005). SPMS typically uses a time-of-flight mass analyzer (TOF-MS) to investigate the different mass-to-charge (m/z) ions simultaneously. However, the laser ionization source could cause a large initial kinetic energy dispersion of ions (Vera et al., 2005), making it difficult for TOF-MS to compensate for the kinetic energy difference through the reflector of TOF-MS, resulting in a low mass resolution of the method. To improve the accuracy of qualitative analysis, the identification of ions in the spectra is improved by organic fragment ions, metal oxide ions, and isotopic ions (Tan et al., 2002). However, these methods have reduced applicability for ions with mass deviations of less than 1 Da. Delayed ion extraction could be an effective method to enhance the resolution of laser ionization mass spectrometry (Kinsel and Johnston, 1989), and this technique has been applied to instruments such as miniSPLAT (Zelenyuk et al., 2015), BAMS (Czerwieniec et al., 2005), ALABAMA (Clemen et al., 2020), and others. Our team has also developed an exponential form of the ion delay extraction technique, which can effectively improve the performance of SPMS in terms of resolution and hit rate (Chen et al., 2020; Li et al., 2018).

Although there have been several studies based on previous SPAMS (Li et al., 2011) to improve the performance – e.g., resolution (Li et al., 2018), hit rate (Chen et al., 2020), and mass accuracy (Chudinov et al., 2019; Zhu et al., 2020) – and while the high-performance single-particle aerosol mass spectrometer (HP-SPAMS) has been applied to the study of particle density (Peng et al., 2021), diesel vehicle exhaust (Su et al., 2021a), and sea salts (Su et al., 2021b), the overall design of HP-SPAMS has not yet been described and characterized. In this study, the performance of HP-SPAMS will be described in detail, and a comparison of the performance with SPAMS will be made. Firstly, the structure and design of the HP-SPAMS are described. Then the detection capability of HP-SPAMS and SPAMS for the number of particles is compared and analyzed in terms of the efficiency of sizing and hit rate. Furthermore, the detection results of the system as it is configured are shown. Finally, the improvement in resolution and sensitivity in relation to the detection results of individual particles by HP-SPAMS and SPAMS are compared and examined.

2 Instruments and methods

HP-SPAMS was designed based on the SPAMS (Li et al., 2011), and its schematic structure is shown in Fig. 1a. Briefly,

the aerosol particles were introduced through an aerodynamic particle concentrator (APC) into an improved aerodynamic lens (ADL) to be focused into a particle beam. The particle size was measured by a scattering system with two higher-power continuous lasers. Chemical information of the particles was obtained by bipolar TOF-MS analysis of ions derived from pulsed-laser ablation and ionization of particles. The photograph of the HP-SPAMS setup is shown in Fig. 1b. The instrument's main body was placed in the upper part of the frame, and the lower part was composed of the power supply, control unit, and pump. The size of the whole machine is 960 mm × 740 mm × 1550 mm, and it weighs 220 kg.

2.1 Aerosol inlet and sizing system

To increase the inlet flow, HP-SPAMS increased the critical orifice diameter from 0.1 to 0.18–0.22 mm, increasing the inlet flux to 0.3–0.5 L min^{-1}, which is greater than the 0.1 L min^{-1} of SPAMS. However, the surplus flow could affect the focusing effect of particles in the aerodynamic lens and could not maintain a suitable vacuum. A scroll pump (IDP-3 Agilent) was supplied at the front of the aerodynamic lens to extract the surplus flow. A separation cone was added below the critical orifice so the particles were not pumped away with the surplus flow (Fig. 1). Due to the difference in inertia between the gas and the particles, 50 % of 50 nm particles and 100 % of 100 nm–1 µm particles entered the separation cone (Zhuo et al., 2021). This structure is like the virtual impactor, which could achieve the concentration of particles, so it is called an aerodynamic particle concentrator (APC). In addition, to analyze large particle sizes, the ADLs were designed (Wang et al., 2005; Wang and McMurry, 2006) and optimized using Fluent 2021 R2 software (ANSYS, Inc.), and the new aerodynamic lens apertures were 5.0, 4.8, 4.4, 4.1, and 3.9 mm. The aerodynamic inlet pressure is in the range of 2.0 ± 0.2 Torr, and the exit nozzle size is 3 mm. The improved inlet system could theoretically transport particles in the range of 100–5000 nm. The theoretical transmission efficiency curve is shown in Fig. S1 in the Supplement, and the experimentally measured time of flight for 150–5400 nm particles is shown in Fig. S2.

Two lasers (500 mW, LaserWave; LWGL 532 nm–500 mW) were used to generate two continuous-wave 532 nm laser beams orthogonally spaced 6 cm apart, which were each focused by a plano-convex lens (PLCX-25.4-51.5-C-532, CVI Laser Optics) into a 300 µm sized spot at the first focus of the ellipsoidal mirror. The scattered light is produced as the particles pass through the laser beam and is focused by the ellipsoidal mirror to the photomultiplier tube (PMT, H10721-110, Hamamatsu) for detection. Compared to SPAMS, the laser power is increased from 75 mW to a maximum of 500 mW, which enhances the intensity of the light scattered by the particles. Furthermore, by optimizing the optical path system and low filtering (1.9 MHz) of the signal of PMT, the background noise level has changed from -9.8 ± 6.4 to -10 ± 0.8 mV, which indicates that the low-pass filtering reduces the influence of stray light (Fig. S3). The whole sizing system was calibrated with standard polystyrene latex (PSL) material, and the formula $d_a = a + bt + ct^2 + dt^3$ was used for particle sizing to meet the accuracy of a wide particle size range. In addition, the HP-SPAMS sizing system could work in the conventional sizing and counting mode but also add a new compensation mode. This mode increased the number of detections of small particles by periodically selecting particles of different particle size segments.

2.2 Aerosol ionization and mass spectrometry

HP-SPAMS uses a diode-pumped Nd, YAG 266 nm (100 Hz, 9 ns pulse width, Centurion Plus, Quantel), that is focused by a UV fused silica plano-convex lens ($f = 175$ mm, SPX026, Newport Corporation) into a 300 µm square uniform spot at the center of the ion source. Compared to the ionized laser of SPAMS, the laser of HP-SPAMS contains two features. One is that the laser frequency has been increased from 20 Hz in SPAMS to 100 Hz. The second is that SPAMS employs a laser with a Gaussian beam, while HP-SPAMS employs a laser with a homogenized spot. The laser beam homogenization gives the spot approximate energy density at different locations, which was shown to improve the repeatability of measurements by Steele et al. (2005)'s research. In addition, the laser adopted air-cooling technology, which does not require circulating water to cool the internal laser system and is suitable for vibration environments such as vehicles and ships, improving the stable operation.

The detailed design of the bipolar TOF-MS is described in detail in previous works (Li et al., 2011, 2018). Briefly, a wide mass range of ion kinetic energy compensation was produced by an exponential pulse delay electric field so that ions of the same mass reached the detector simultaneously to achieve an improved resolution. Another advantage of using the pulse delay extraction technique instead of DC extraction is that it eliminates the problem that charged aerosol particles can deflect in the mass spectrometry electric field conditions, thus improving the instrument's hit rate (Chen et al., 2020; Clemen et al., 2020). Calibration of each spectrum after the resolution improvement could ensure a mass deviation within ±0.024 Da (Zhu et al., 2020).

The inhomogeneity of the components of the aerosol particles could result in large differences in the signal response of the microchannel plate detector (1.8 ns single ion response, half-peak width), which may reach a maximum of 20 V and a minimum of only a few millivolts. Therefore, it was not easy to achieve such a high dynamic range acquisition with a single channel using a conventional analog-to-digital conversion (ADC) acquisition card. HP-SPAMS employed a four-channel data acquisition technique, with positive or negative ion signals being acquired with two channels, the same tech-

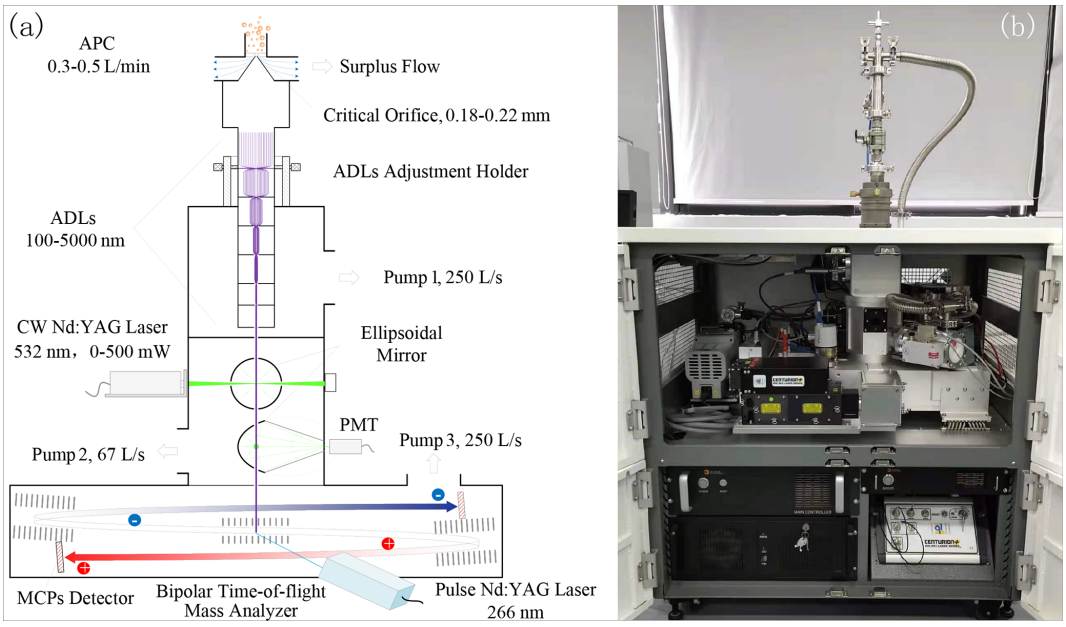

Figure 1. Schematic diagram and photograph of the HP-SPAMS instrument. **(a)** The aerosol particles were introduced through an APC into an improved aerodynamic lens (ADL) to be focused into a particle beam. A scattering system measured the particle size with two higher-power continuous lasers (532 nm). Particle chemical components were obtained by bipolar time-of-flight mass spectrometry analysis of ions derived from a pulsed-laser (266 nm) ablation and ionization of particles. **(b)** The instrument's main body was placed in the upper part of the frame, and the lower part was composed of the power supply, control unit, and pump.

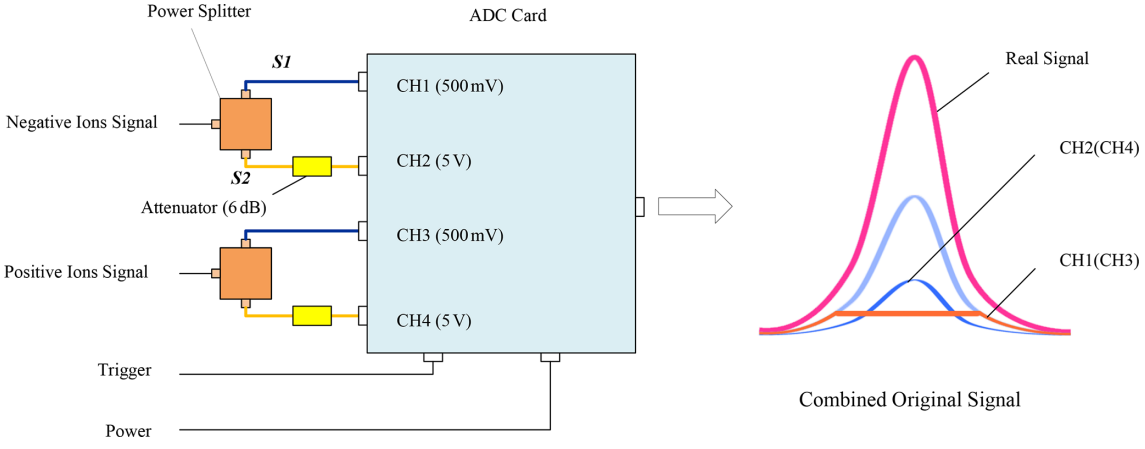

Figure 2. Schematic diagram of the working principle of multi-channel data acquisition. The ion signals were acquired separately using two channels with different ranges (500 mV and 5 V) of the ADC (8-bit). Finally, the real signal intensity was obtained by synthesizing the signals of two channels through software algorithms, and the dynamic acquisition range reached 4 mV–20 V.

nique that is used in the ALABAMA and ATOFMS instruments (Clemen et al., 2020; Pratt et al., 2009). As in Fig. 2, a signal was split into two similar signals (S1 and S2) with half attenuation through a power splitter (Mini-circuit, ZFRSC-42+). S1 was acquired by the CH1 channel (2–500 mV) of the ADC card (Acqiris, U5309-CH4, 8bit, 1GS/s), while S2 was acquired by the CH2 channel (20 mV–5 V) after passing through an attenuator (6 dB). The data acquired by CH1 and CH2 were combined with the algorithm to generate the real ion signal. Therefore, the dynamic acquisition range of 4 mV–20 V using the four-channel data acquisition method enabled HP-SPAMS to represent the original peaks of the spectrum more accurately on the one hand and to improve the identification of trace components on the other hand. Although it is theoretically possible to achieve such a dynamic range using a high-bit data acquisition card, ADC acquisition cards for SPMS typically perform only one acquisition for a single particle, which made the ADC acquisition card unable

to suppress noise by accumulating acquisitions, and thus it cannot achieve the theoretical dynamic range in practical applications.

2.3 Experimental materials and tools

Standard particle size (100–5000 nm) polystyrene latex microspheres (PSLs), dioctyl sebacate (DOS), sodium chloride (NaCl), and ammonium sulfate (AS) were separately dissolved in an aqueous solution to produce aerosols using a single-jet atomizer (TSI 9302). The resulting aerosol particles were passed through a diffusion dryer to form polydisperse aerosol particles (Fig. 3a). To obtain monodisperse particles, particles of different sizes (100–3000 nm) were screened using the aerodynamic aerosol classifier (AAC, Cambustion), and the concentration of particles was measured by a condensation particle counter (CPC 3775, TSI). Air sampling was performed in the production workshop of Hexin Instruments (Guangzhou Science City, Guangzhou), where daily activities such as instrument commissioning and assembly were performed. Indoor air samples were fed through a carbon-black tube into the DUST METER (flow rate 3 L min^{-1}, TSI DUSTTRAK II 8530), a scanning mobility particle sizer spectrometer (SMPS, flow rate 0.3 L min^{-1}, TSI 3321), SPAMS (0.1 L min^{-1}, Guangzhou Hexin Instrument Co., Ltd.), and HP-SPAMS (0.3 L min^{-1}) (Fig. 3b). In order to compare the detection capabilities of the two instruments at low concentrations (1–5 µg m^{-3}), laboratory air samples collected by SPAMS and HP-SPAMS were diluted 40 times with an aerosol diluter (Shenzhen Zhanye Dahong Technology Co., equipped with a 3 L min^{-1} pump), from 60 to 180 µg m^{-3}.

In order to characterize the performance of the instrument, the scattering efficiency and hit rate associated with the instrument are defined. The scattering efficiency of particles is defined as the ratio of the response pulse count of the photomultiplier tube to the total number of injected particles. It can be described by the equation $E_s = N_s/(C_{CPC} \times Q)$, where N_s is the response pulse count of the photomultiplier tube (pulse s^{-1}), C_{CPC} is the particle number concentration by the CPC (particle cm^{-3}), and Q is the flow rate of the sampling inlet (cm^3 s^{-1}). The hit rate is defined as the ratio of the number of particles with mass spectra to the number of sizing particles. It can be described by the equation $HR = N_{mass}/N_{sizing}$, where N_{sizing} is the number of sizing particles, which refers to the number of particles accurately measured by the sizing system when the ionizing laser can be emitted, and N_{mass} is the number of particles with mass spectra. In addition, both HP-SPAMS and SPAMS operate at laser energies of about 0.5 mJ per pulse during the experiments, and lower fluence can reduce the fragmentation of organic molecules (Silva and Prather, 2000).

3 Results and discussion

3.1 Improved efficiency and quantity of particle detection

The scattering efficiencies of HP-SPAMS and SPAMS for AS, DOS, NaCl, and PSLs particles were compared (Fig. 4). The results show the scattering efficiencies of aerosol in the particle size range of 100–3000 nm in both SPMSs, where legend PMT1 and PMT2 represent the scattering efficiencies of the two photomultiplier tubes of SPAMS, respectively. HP-PMT1 and HP-PMT2 are the scattering efficiencies of the two photomultiplier tubes of the HP-SPAMS scattering efficiency. The results showed that the scattering efficiency of HP-SPAMS was higher than that of SPAMS for all the investigated aerosol particles. Moreover, the HP-SPAMS and SPAMS scattering efficiencies at PMT1 were higher than that at PMT2 because the particles underwent dispersive motion after passing through the aerodynamic lens, although the dispersion was very small. Comparing the samples with different particle morphologies, the scattering efficiencies of spherical DOS (shape factor $\chi \approx 1$) and PSL ($\chi = 1$) particles were higher than those of non-spherical AS ($\chi \approx 1.1$) and NaCl ($\chi = 1.69$–6.27) particles; in particular, the scattering efficiency of the DOS particles in the range of 300–1000 nm was almost 100 % (Tavakoli and Olfert, 2014; Zelenyuk et al., 2006). This is due to the fact that, for irregular particles, there is a force perpendicular to the direction of gas motion, while, for spherical particles, this force is zero, resulting in greater dispersion of non-spherical particles after passing through the lens system (Liu et al., 1995).

Two aspects influenced the enhancement of HP-SPAMS scattering efficiency. On the one hand, it was due to the improved transmission efficiency of the inlet system, especially the adoption of a larger critical orifice, resulting in a lower loss rate of particles before entering the aerodynamic lens (Cahill et al., 2014). On the other hand, the enhancement of the power of the continuous laser and the reduction in the background noise level improved the ability of the sizing system to detect small particles and particles at the edge of the Gaussian beam. In addition, HP-SPAMS made it possible to increase the number of incoming particles by a factor of 3–5 by introducing the APC device, which was determined by the diameter of the critical orifice. Therefore, the number of particles detected by the HP-SPAMS sizing system could be greatly increased, and this is related to the particle size and the type of the particles.

Figure 5 shows the hit rate curves of HP-SPAMS and SPAMS for different particle size segments of aerosols in PSLs and workshop air, respectively. Due to the limited number of large particles collected by SPAMS for air, the hit rate of SPAMS for particles larger than 1250 nm in size may not be accurate. As seen from Fig. 5, the hit rate of HP-SPAMS for PSLs could be maintained in the range of 200–3000 nm at 80 % to 100 % for PSLs, while the SPAMS was within 20 %.

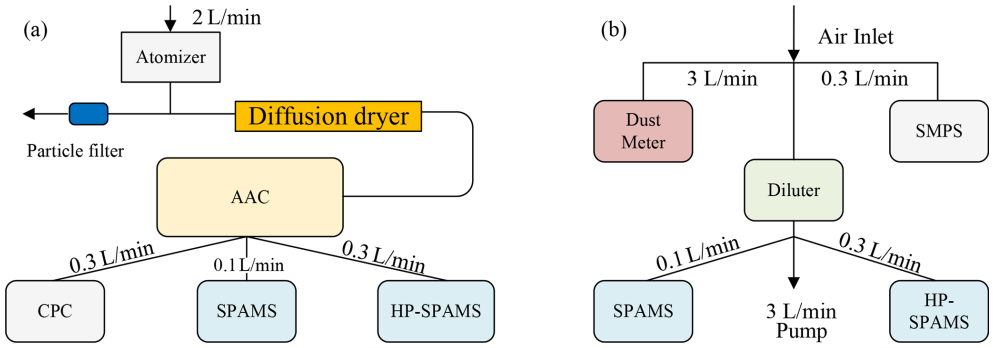

Figure 3. Standard sample and laboratory air experiment diagram. **(a)** The atomizer produced standard particles (100–5000 nm) and dried them with a diffusion dryer. The monodisperse particles (100–3000 nm) were screened using the aerodynamic aerosol classifier (AAC, Cambustion). Moreover, the monodisperse particles are measured by a condensation particle counter (CPC 3775, TSI), SPAMS, and HP-SPAMS. **(b)** Air samples were fed through a carbon-black tube into the dust meter, SMPS, SPAMS, and HP-SPAMS, respectively. To further compare the detection capability of the instruments at low concentrations, the fraction of the samples fed by SPAMS and HP-SPAMS was diluted 40 times by an aerosol diluter.

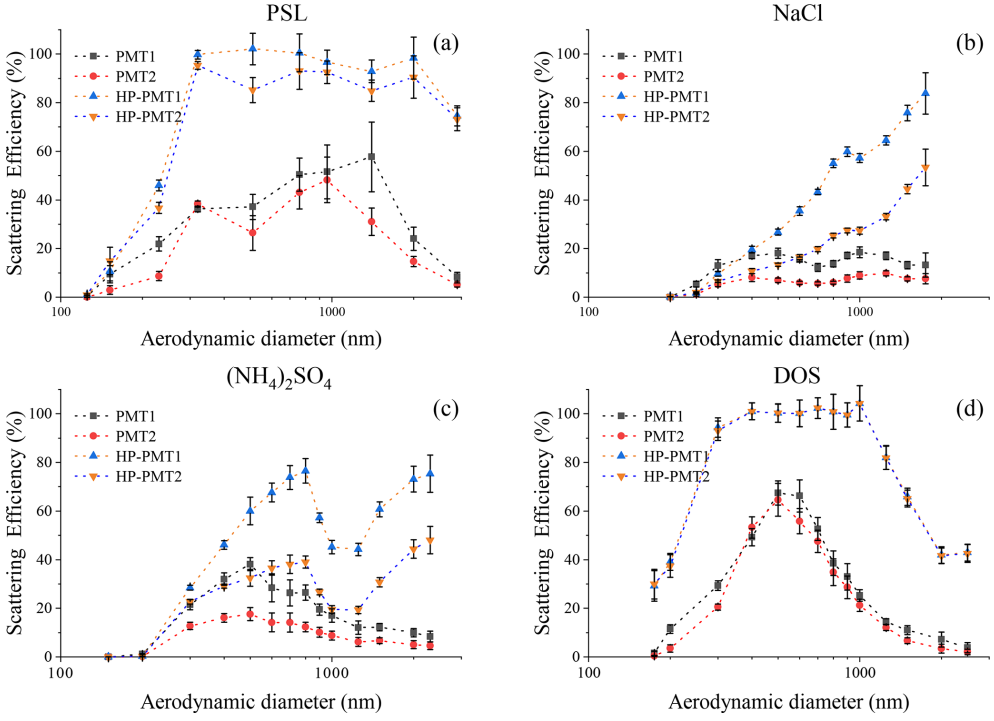

Figure 4. Comparison of HP-SPAMS and SPAMS for different particle-sizing scattering efficiencies ranging from 100–3000 nm. The PMT1 and PMT2 represent the scattering efficiency of the two photomultiplier tubes of SPAMS, respectively, and HP-PMT1 and HP-PMT2 are the scattering efficiency of the two photomultiplier tubes of HP-SPAMS.

In the range of 100 to 500 nm, the hit rate of both instruments decreases with smaller particle size. This is because the aerosol produced by the atomizer will be charged (Chen et al., 2020), and when the aerosol is under the action of the direct-current (DC) electric field of SPAMS, the particles will be deflected in the extraction region of the TOF analyzer. On the contrary, HP-SPAMS showed a better hit rate due to the use of delayed ion extraction (Chen et al., 2020); a similar finding was reported by Clemen et al. (2020). It could be observed from the particle size segment of less than 500 nm that, for SPAMS, the air hit rate was higher than the hit rate of PSLs due to the relatively low charge of particles in the environment (He et al., 2020). There was a decrease in air particles larger than 1000 nm in both HP-SPAMS and SPAMS due to the increase in non-spherical particles affecting the focusing of ADLs. Besides the effect of particle trajectory

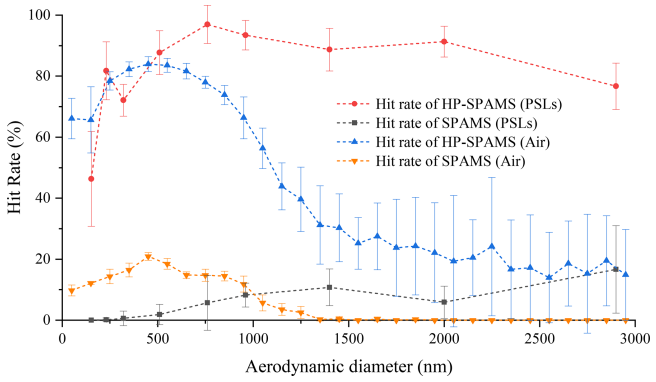

Figure 5. The HP-SPAMS and SPAMS hit rate plots for PSLs and air at different particle sizes. For measuring both PSLs and air, HP-SPAMS had a higher hit rate than SPAMS. For PSL particles, the hit rate of HP-SPAMS could be maintained in the range of 200–3000 nm at 80 % to 100 % for PSLs, while the SPAMS was within 20 %.

and focus, the hit rate was also influenced by the characteristics of the ablation–ionization laser. Because the components of various particles differed, the particles showed different laser energy absorption cross-sections and required different laser energy thresholds to produce ions (Thomson et al., 1997), and it was also found in the experiment that pure NaCl, NaCl, and DOS particles do not form ions at an energy rate of 0.5 mJ per pulse. Therefore, even for the same particle, differences in energy density at the edges and center of the SPAMS non-uniform Gaussian beam could cause the particles to not be ionized.

Further, to compare the instruments' improvement in terms of particle detection quantity, the SMPS, DUST METER, HP-SPAMS, and SPAMS instruments collected and analyzed the air samples simultaneously (Fig. 3b). The samples collected by SPAMS and HP-SPAMS were the samples after the diluter (40 times dilution). The variation in particle concentration during 24 h of continuous monitoring of air samples is shown in Fig. 6, where HP-PMT1-2 refers to the number of particles passing through the two laser beams without particle catch-up. The SMPS monitoring concentration results showed a peak around 12:00 and 16:00 local time (UTC+8), which may be due to some aerosol particles generated in the workshop, and particle concentrations continued to decline until the following morning. Pearson correlation analysis between SMPS concentration, $PM_{2.5}$ concentration, and the data of PMT detection by HP-SPAMS was performed (Table 1). A significant correlation was found between HP-SPAMS measurement data and DUST METER (Pearson correlation > 0.97). The correlation coefficient between SMPS and DUST METER and HP-SPAMS was lower (Pearson correlation > 0.76) due to the ability of SPMS to measure particles below 100 nm, leading to a lower correlation of particles due to the influence of small particles.

The statistical analyses of SMPS, SPAMS, and HP-SPAMS particle sizes are detailed in Fig. 7. The SMPS is the data after averaging 24 h sampling points (634 cycles), and HP-SPAMS and SPAMS are the particle size measurement and hit statistical particle distribution, respectively. The peak particle sizes of the three instruments were 88.2, 300, and 380 nm for SMPS, HP-SPAMS, and SPAMS, respectively. HP-SPAMS was more efficient than SPAMS in measuring particles in the small particle size range, which is consistent with the results of the test standard particle (Fig. 4). In an environment with $PM_{2.5}$ concentrations of 50–200 $\mu g\,m^{-3}$ (Fig. 6) and after dilution of 40-fold, the number of sizing particles measured by the two instruments was 1 281 846 (2.8 particles per milliliter on average,) and 146 600 (1.02 particles per milliliter on average), respectively, indicating that the average particle detection capability was about 8.7 times improved by improving the inlet system and the sizing system. The numbers of comparison hit particles were 1 002 141 (78.2 % hit rate) and 20 943 (14.3 % hit rate). Figure S4 shows the curve of the number of particle sizing and hit as a function of time. The results in Fig. S4 also show that, even in a low $PM_{2.5}$ concentration of 1 $\mu g\,m^{-3}$, the instrument still detects an average of about 5.04 hit particles per second, which is related to atmospheric particles' composition and mixing state. The enhancement of the number of detected particles is very important for low $PM_{2.5}$ concentrations, improving the temporal resolution of aerosol characterization, such as North or South Pole aerosols, upper-tropospheric cloud nuclei, and coupling with SMPS instruments.

3.2 Mass resolution and detection sensitivity

Figure 8 shows the resolution of positive and negative ions for detecting environmental particles for HP-SPAMS and SPAMS. To ensure the accuracy of the resolution calculation, spectrum peaks with peak intensities above 100 mV and unsaturated spectrum peaks (< 20 V or < 5 V) were selected. It can also be seen from Fig. 8 that the resolution of HP-SPAMS using exponential pulse delay extraction is, on average, 2–3 times better than that of the DC extraction SPAMS (Li et al., 2018), and the average resolution is up to 2500 (full width at half maximum) at m/z 208. This resolution is better than that of instruments of the same type, such as LAAPTOF (600) and A-ATOFMS (1072) (Gemayel et al., 2016; Pratt et al., 2009). The better resolution of HP-SPAMS is due to the exponential pulse delay extraction technique that compensates for the different ion kinetic energy dispersion and solves the problem of the difference in ion generation time due to the laser emission period (several nanoseconds). Of course, not all the peaks of HP-SPAMS have very good resolution due to the various components of the particles.

In addition, Fig. 8 shows that the number of HP-SPAMS peaks was significantly higher than that of SPAMS, especially for m/z above 100, which indicates that HP-SPAMS

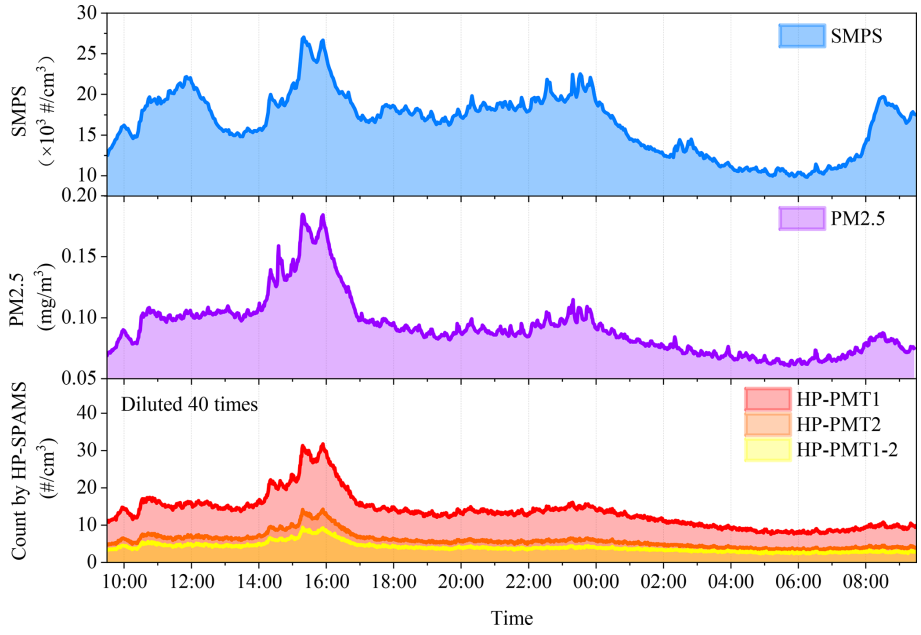

Figure 6. The SMPS, DUST METER, and HP-SPAMS instrument air collection number concentration temporal plot curve (local time, UTC+8). SMPS measured particle number concentrations from 10 to 760 nm. $PM_{2.5}$ concentrations ranged from 50 to 180 $\mu g\,m^{-3}$ and reached a maximum concentration of 180 $\mu g\,m^{-3}$ in the afternoon. HP-SPAMS demonstrated particle number concentrations detected at a 40-fold dilution.

Table 1. Pearson's correlation* analysis of SMPS concentrations, $PM_{2.5}$ concentrations, and the number of particles detected by HP-SPAMS.

	SMPS	$PM_{2.5}$	HP-PMT1	HP-PMT2	HP-PMT1-2
SMPS	1	0.818	0.815	0.786	0.768
$PM_{2.5}$		1	0.984	0.982	0.977
HP-PMT1			1	0.997	0.993
HP-PMT2				1	0.999
HP-PMT1-2					1

* Correlation is significant at the 0.01 level (two-tailed).

detects more ions and has better particle component detection sensitivity than SPAMS. It is noteworthy that the ion spectrum peaks with peak intensities of less than 100 mV were not yet showed in the figure. The increase in the spectral peaks may be due to the following effects: (1) the increase in resolution increased the signal intensity collected by the ADC; (2) it could increase the collision of electrons, ions, and neutral components during the delay time (Reinard and Johnston, 2008); and/or (3) the particles were better ionized under a uniform laser beam, even if they fell in different areas of the spot (Steele et al., 2005).

The improved resolution could efficiently distinguish between ions with similar masses but different elemental compositions. Table 2 lists the required theoretical resolution at 50 % discrimination of similar ions with m/z less than 60 Da. HP-SPAMS could distinguish most of the interferences between metal ions and organic fragment ions, except for Mg^+ (23.985) and C_2^+ (24.000). In addition, HP-SPAMS distinguished the interference between some organic fragment ions. Previously, metal ions were successfully distinguished by metal oxide ions or isotopic peaks (Snyder et al., 2009; Zhou et al., 2020), such as the identification of vanadium-containing particles by V^+ (51) and VO^+ (67) ions and of iron-containing particles by the peak area ratio Fe (56) / Fe (54) > 3. These methods can identify the particles containing metals, while some metal-containing particles will be ignored due to the high percentage of organic fragment ions. Figure 9 shows two metal-containing particles, the K–Cu-amine-containing particles (Fig. 9a) and Fe-amine-aged particles (Fig. 9b). In Fig. 9a, it can be observed that there are two peaks of V^+ (50.94396) and $C_4H_3^+$ (51.02348) at m/z 51, which could indicate that the particle contained metallic vanadium. Likewise, Fe^+ (55.93494) and $C_4H_8^+$ (56.06260) could be distinguished in Fig. 9b, and the isotopic peaks Fe^+ (53.93961) and Fe^+ (56.93539) could be identified. Therefore, the improved resolution of HP-SPAMS

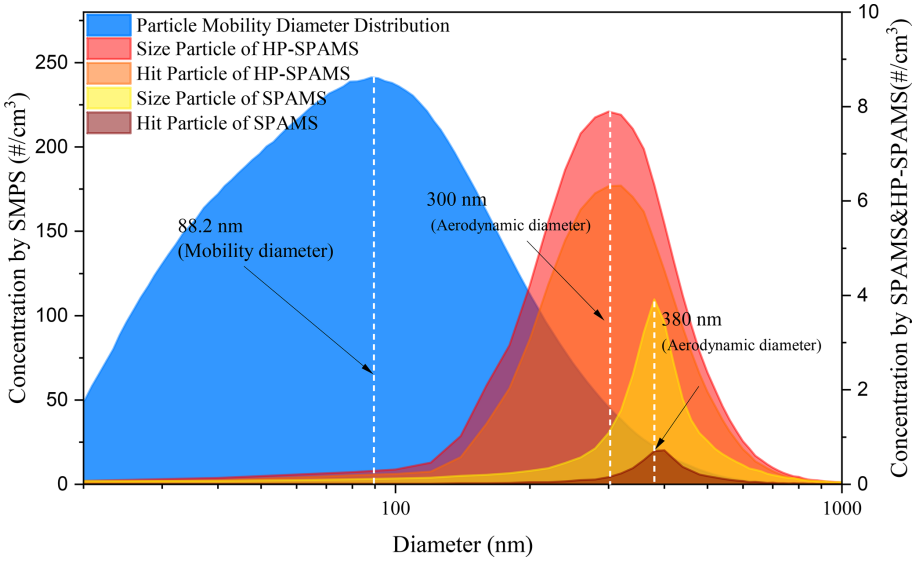

Figure 7. Particle size distribution of SPMS, HP-SPAMS, and SPAMS detection during 24 h. The peak particle sizes of the three instruments were 88.2, 300, and 380 nm, respectively. The number of sizing particles measured by the two instruments was 1 281 846 and 146 600, respectively. The number of comparison hit particles was 1 002 141 (78.2 % hit rate) and 20 943 (14.3 % hit rate).

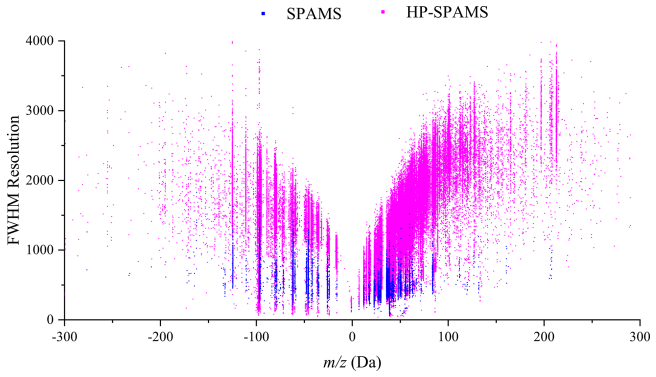

Figure 8. HP-SPAMS and SPAMS positive and negative ion resolution scatter plot.

to better monitor metal-containing particles will help to more accurately investigate the atmospheric chemical processes and pollution involved in metals in atmospheric particles.

3.3 Analysis of lead-containing particles

The performance of HP-SPAMS is usually more sensitive and accurate for analyzing aerosol particles compared to the SPAMS, making it possible to obtain valid data for analysis even at low concentrations. For example, the lead-containing particles were compared and analyzed in Fig. 7. By screening the particles containing m/z 206, 207, and 208, along with those not containing m/z 202, the number of lead-containing particles detected by HP-SPAMS and SPAMS was obtained as 7955 and 55, respectively. The increase in the number of lead-containing particles detected was due to the increase in the overall number of particles detected by a factor of about 47.8 (1 002 141 / 20 943) and due to the increase in the detection sensitivity of individual particles.

A total of 50 lead-containing particles detected by SPAMS and HP-SPAMS were randomly selected for each from the results of the above screening, and each particle's m/z is shown in Fig. 10a and b. It could also be observed that the lead-containing particles detected by HP-SPAMS have more spectral peaks, which could be related to the enhancement of the particle ionization and delayed elicitation techniques and due to the use of high-dynamic-range data acquisition, which could acquire a minimum signal of 4 mV. The high-dynamic-range data acquisition allowed more valid mass spectral peaks, especially for some large m/z of organics. The as-improved resolution could completely distinguish adjacent mass spectral peaks, which helps improve the accuracy of isotope ratio measurements. Statistical analysis of the relative peak areas of $^{206}Pb^+$ vs. $^{208}Pb^+$ was performed for all SPAMS- and HP-SPAMS-acquired Pb-containing particles (Fig. 10c and d). A linear fit to the relative peak areas showed better linearity of the isotopic ratios for HP-SPAMS ($R^2 = 0.92$). In addition, the isotope ratio $^{208}Pb^+ / ^{206}Pb^+$ is 1.933, which is a deviation of about 11.07 % from the theoretical isotope ratio for lead ($^{208}Pb^+ / ^{206}Pb^+ = 2.174$). In summary, the higher resolution of HP-SPAMS, as well as the improved dynamic range of the data acquisition with peak intensities up to 20 V, makes HP-SPAMS more prominent for the use of isotopic identification, such as source apportionment or mineral identification (Marsden et al., 2018; Souto-Oliveira et al., 2018; Su et al., 2023).

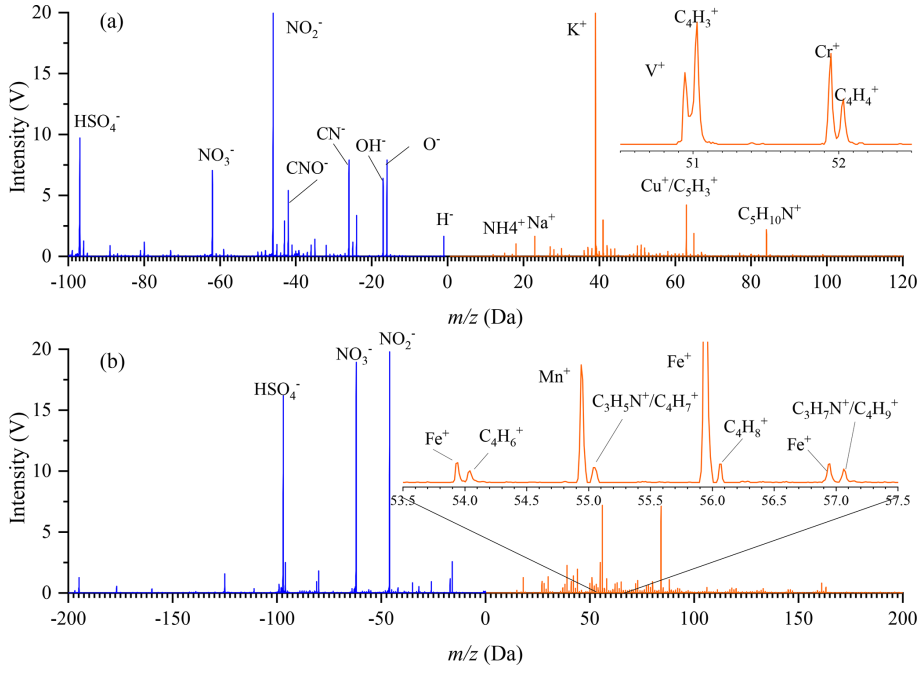

Figure 9. Example particles of high-resolution spectra **(a)** K–Cu-amine-containing particles **(b)** Fe-amine aged particles.

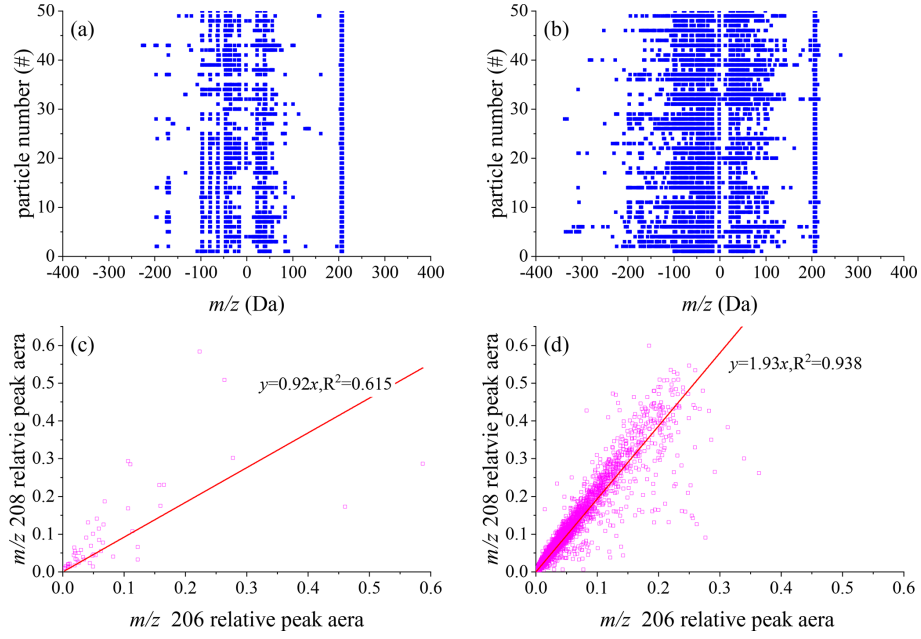

Figure 10. Panels **(a)** and **(b)** show the scatter plots of the mass-to-charge ratios of the ions of the lead-containing particles from SPAMS and HP-SPAMS, respectively. Panels **(c)** and **(d)** showed the scatter plots of the relative peak areas of $^{208}Pb^+$ vs. $^{206}Pb^+$ for the lead-containing particles from SPAMS and HP-SPAMS, respectively.

4 Conclusions

The high-performance single-particle aerosol mass spectrometer (HP-SPAMS) was described with an integrated aerodynamic particle concentration device; dual-polarity exponential pulse delay elicitation; multi-channel data acquisition; and an improved aerodynamic lens, sizing system, and ionization system, making the instrument significantly more efficient in the quantitative detection of particles. Moreover, the accuracy and sensitivity of the quantification of individual particles were also improved compared to SPAMS.

Table 2. Resolution required and achieved for 50 % separation of similar mass number ions with mass numbers less than 60 Da that may be generated by HP-SPAMS.

Ions	Similar ions	R^a	R^b	Ions	Similar ions	R^a	R^b
Mg^+ (23.985)	C_2^+ (24.000)	2250	603 ± 198	Ti^+ (47.948)	C_4^+ (48.000)	1300	1210 ± 273
Al^+ (26.981)	$C_2H_3^+$ (27.023)	940	746 ± 159	Cr^+ (49.946)	$C_3N^+/C_4H_2^+$ (50.003/50.016)	1100	1321 ± 223
CHO^+ (29.003)	$C_2H_5^+$ (29.039)	1150	829 ± 214	V^+ (49.947)	$C_4H_3^+/C_3HN^+$ (51.024/51.011)	920	1411 ± 228
$NO^+/CHOH^+$ (29.998/30.011)	$CH_4N^+/C_2H_6^+$ (30.034/30.05)	1210	755 ± 284	Cr^+ (51.941)	$C_4H_4^+$ (52.031)	800	1402 ± 282
P^+ (30.974)	CH_3O^+ (31.018)	1010	946 ± 232	Fe^+ (53.940)	$C_4H_6^+$ (54.047)	790	1421 ± 284
K^+ (38.964)	$C_3H_3^+$ (39.024)	950	946 ± 306	Mn^+ (54.938)	$C_3H_5N^+/C_4H_7^+$ (55.042/55.055)	770	1368 ± 355
Ca^+ (39.964)	$C_3H_4^+$ (40.031)	850	1018 ± 314	Fe^+ (55.935)	$C_4H_8^+$ (56.063)	630	1435 ± 299
K^+ (40.962)	$C_3H_5^+$ (41.039)	820	1081 ± 298	$CaOH^+$ (56.965)	$C_4H_9^+/C_3H_7N^+$ (57.070/57.058)	780	1300 ± 356
$CHNO^+/CH_3CO^+$ (43.006/43.018)	$C_3H_7^+$ (43.055)	1280	935 ± 263	Ni^+ (57.935)	$C_3H_8N^+/C_4H_{10}^+$ (58.066/58.078)	700	1579 ± 203
SiO^+/Ca^+ (43.972/43.955)	$C_2H_6N^+$ (39.963)	800	1242 ± 226	C_5^+ (60.000)	$C_3H_{10}N^+$ (60.081)	1050	1444 ± 420

[a] Resolution required for 50 % separation of two similar ion peaks. [b] Resolution statistics of HP-SPAMS at different mass-to-charge ratios.

Comparative analysis between HP-SPAMS and SPAMS showed that the increased inlet flow rate as a result of adding the APC could enhance the particle number concentration by a factor of 3–5. Combined with the improved aerodynamic lens and sizing system, the transfer and measurement of 100–5000 nm particles are achieved. For spherical particles, the sizing transfer efficiency is almost 70 %–100 % in the 300–3000 nm range. The hit rate was improved by factor of about 5 by as a result of reducing the deflection of charged particle beams through the pulse delay extraction technique. The results of atmospheric aerosol analysis showed that the correlation between the number of particles detected by HP-SPAMS and the $PM_{2.5}$ mass concentration reached 0.97 (Pearson correlation), and its detection efficiency was higher than SPAMS for small particle sizes. The total number of particles effectively detected was improved by approximately 47.8 times.

For the composition detection of individual particles, HP-SPAMS improved the resolution of the method by 2–3 times and could distinguish most of the metal ions and organic fragment ions with more accurate isotopic ratios, enabling this approach to improve the accuracy of aerosol component identification and aerosol sources. In addition, although the sensitivity of HP-SPAMS to analyzed individual particles cannot be quantified, it can be inferred that HP-SPAMS can improve the sensitivity toward individual particle detection by improving the number of particles detected (such as for lead-containing particles) and the chance of detection of ions with a high mass-to-charge ratio.

Code and data availability. Data and code are available on request from Lei Li (lileishdx@163.com).

Supplement. The supplement related to this article is available online at: https://doi.org/10.5194/amt-17-1037-2024-supplement.

Author contributions. LL and XD designed the study, and XD, QX, QH, and XuaL performed the experiments and data analysis. JY, ZH, and JW provided engineering support. ZZ, ZH, and WG provided instrument resources. XD, XueL, and LL wrote and revised the paper. LL and ZZ are project administrators.

Competing interests. The contact author has declared that none of the authors has any competing interests.

Disclaimer. Publisher's note: Copernicus Publications remains neutral with regard to jurisdictional claims made in the text, published maps, institutional affiliations, or any other geographical representation in this paper. While Copernicus Publications makes every effort to include appropriate place names, the final responsibility lies with the authors.

Special issue statement. This article is part of the special issue "Dust aerosol measurements, modeling and multidisciplinary effects (AMT/ACP inter-journal SI)". It is not associated with a conference.

Acknowledgements. We would like to thank Zhang Guohua and Hu Ligang for their help in writing this article.

Financial support. This research has been supported by the National Key Research And Development Program For Young Scientists (grant no. 2022YFF0705400).

Review statement. This paper was edited by Lucia Mona and reviewed by five anonymous referees.

References

Cahill, J. F., Darlington, T. K., Wang, X., Mayer, J., Spencer, M. T., Holecek, J. C., Reed, B. E., and Prather, K. A.: Development of a High-Pressure Aerodynamic Lens for Focusing Large Particles (4–10 µm) into the Aerosol Time-of-Flight Mass Spectrometer, Aerosol Sci. Tech., 48, 948–956, https://doi.org/10.1080/02786826.2014.947400, 2014.

Cahill, J. F., Fei, H., Cohen, S. M., and Prather, K. A.: Characterization of core-shell MOF particles by depth profiling experiments using on-line single particle mass spectrometry, Analyst, 140, 1510–1515, https://doi.org/10.1039/c4an01913j, 2015.

Chen, S.-C., Tsai, C.-J., Wu, C.-H., Pui, D. Y. H., Onischuk, A. A., and Karasev, V. V.: Particle loss in a critical orifice, J. Aerosol Sci., 38, 935–949, https://doi.org/10.1016/j.jaerosci.2007.06.010, 2007.

Chen, Y., Kozlovskiy, V., Du, X., Lv, J., Nikiforov, S., Yu, J., Kolosov, A., Gao, W., Zhou, Z., Huang, Z., and Li, L.: Increase of the particle hit rate in a laser single-particle mass spectrometer by pulse delayed extraction technology, Atmos. Meas. Tech., 13, 941–949, https://doi.org/10.5194/amt-13-941-2020, 2020.

Chudinov, A., Li, L., Zhou, Z., Huang, Z., Gao, W., Yu, J., Nikiforov, S., Pikhtelev, A., Bukharina, A., and Kozlovskiy, V.: Improvement of peaks identification and dynamic range for bi-polar Single Particle Mass Spectrometer, Int. J. Mass Spectrom., 436, 7–17, https://doi.org/10.1016/j.ijms.2018.11.013, 2019.

Clemen, H.-C., Schneider, J., Klimach, T., Helleis, F., Köllner, F., Hünig, A., Rubach, F., Mertes, S., Wex, H., Stratmann, F., Welti, A., Kohl, R., Frank, F., and Borrmann, S.: Optimizing the detection, ablation, and ion extraction efficiency of a single-particle laser ablation mass spectrometer for application in environments with low aerosol particle concentrations, Atmos. Meas. Tech., 13, 5923–5953, https://doi.org/10.5194/amt-13-5923-2020, 2020.

Czerwieniec, G. A., Russell, S. C., Lebrilla, C. B., Coffee, K. R., Riot, V., Steele, P. T., Frank, M., and Gard, E. E.: Improved sensitivity and mass range in time-of-flight bioaerosol mass spectrometry using an electrostatic ion guide, J. Am. Soc. Mass Spectrom., 16, 1866–1875, https://doi.org/10.1016/j.jasms.2005.06.013, 2005.

Gemayel, R., Hellebust, S., Temime-Roussel, B., Hayeck, N., Van Elteren, J. T., Wortham, H., and Gligorovski, S.: The performance and the characterization of laser ablation aerosol particle time-of-flight mass spectrometry (LAAP-ToF-MS), Atmos. Meas. Tech., 9, 1947–1959, https://doi.org/10.5194/amt-9-1947-2016, 2016.

He, Y., Gu, Z., Lu, W., Zhang, L., Zhang, D., Okuda, T., and Yu, C. W.: Charging states on atmospheric aerosol particles affected by meteorological conditions, Particuology, 52, 1–9, https://doi.org/10.1016/j.partic.2019.12.007, 2020.

Hwang, T.-H., Kim, S.-H., Kim, S. H., and Lee, D.: Reducing particle loss in a critical orifice and an aerodynamic lens for focusing aerosol particles in a wide size range of 30 nm–10 µm, J. Mech. Sci. Technol., 29, 317–323, https://doi.org/10.1007/s12206-014-1238-4, 2015.

Jost, H.-J., Drdla, K., Stohl, A., Pfister, L., Loewenstein, M., Lopez, J. P., Hudson, P. K., Murphy, D. M., Cziczo, D. J., Fromm, M., Bui, T. P., Dean-Day, J., Gerbig, C., Mahoney, M. J., Richard, E. C., Spichtinger, N., Pittman, J. V., Weinstock, E. M., Wilson, J. C., and Xueref, I.: In-situ observations of mid-latitude forest fire plumes deep in the stratosphere, Geophys. Res. Lett., 31, L11101, https://doi.org/10.1029/2003gl019253, 2004.

Kinsel, G. R. and Johnston, M. V.: Post source pulse focusing: a simple method to achieve improved resolution in a time-of-flight mass spectrometer, Int. J. Mass Spectrom., 91, 157–176, https://doi.org/10.1016/0168-1176(89)83006-x, 1989.

Li, L., Huang, Z., Dong, J., Li, M., Gao, W., Nian, H., Fu, Z., Zhang, G., Bi, X., Cheng, P., and Zhou, Z.: Real time bipolar time-of-flight mass spectrometer for analyzing single aerosol particles, Int. J. Mass Spectrom., 303, 118–124, https://doi.org/10.1016/j.ijms.2011.01.017, 2011.

Li, L., Liu, L., Xu, L., Li, M., Li, X., Gao, W., Huang, Z., and Cheng, P.: Improvement in the Mass Resolution of Single Particle Mass Spectrometry Using Delayed Ion Extraction, J. Am. Soc. Mass Spectrom., 29, 2105–2109, https://doi.org/10.1007/s13361-018-2037-4, 2018.

Liu, P., Ziemann, P. J., Kittelson, D. B., and McMurry, P. H.: Generating Particle Beams of Controlled Dimensions and Divergence: I. Theory of Particle Motion in Aerodynamic Lenses and Nozzle Expansions, Aerosol Sci. Tech., 22, 293–313, https://doi.org/10.1080/02786829408959748, 1995.

Liu, Z., Lu, X., Feng, J., Fan, Q., Zhang, Y., and Yang, X.: Influence of Ship Emissions on Urban Air Quality: A Comprehensive Study Using Highly Time-Resolved Online Measurements and Numerical Simulation in Shanghai, Environ. Sci. Technol., 51, 202–211, https://doi.org/10.1021/acs.est.6b03834, 2017.

Marsden, N. A., Flynn, M. J., Allan, J. D., and Coe, H.: Online differentiation of mineral phase in aerosol particles by ion formation mechanism using a LAAP-TOF single-particle mass spectrometer, Atmos. Meas. Tech., 11, 195–213, https://doi.org/10.5194/amt-11-195-2018, 2018.

McNeill, V. F.: Atmospheric Aerosols: Clouds, Chemistry, and Climate, Annu. Rev. Chem. Biomol. Eng., 8, 427–444, https://doi.org/10.1146/annurev-chembioeng-060816-101538, 2017.

Murphy, D. M.: The design of single particle laser mass spectrometers, Mass Spectrom. Rev., 26, 150–165, https://doi.org/10.1002/mas.20113, 2007.

Murphy, D. M., Cziczo, D. J., Froyd, K. D., Hudson, P. K., Matthew, B. M., Middlebrook, A. M., Peltier, R. E., Sullivan, A., Thomson, D. S., and Weber, R. J.: Single-particle mass spectrometry of tropospheric aerosol particles, J. Geophys. Res.-Atmos., 111, D23S32, https://doi.org/10.1029/2006jd007340, 2006.

Noble, C. A. and Prather, K. A.: Real-time single particle mass spectrometry: a historical review of a quarter century of the chemical analysis of aerosols, Mass Spectrom. Rev., 19, 248–274, https://doi.org/10.1002/1098-2787(200007)19:4<248::AID-MAS3>3.0.CO;2-I, 2000.

Peng, L., Li, L., Zhang, G., Du, X., Wang, X., Peng, P., Sheng, G., and Bi, X.: Technical note: Measurement of chemically resolved volume equivalent diameter and effective density of particles by AAC-SPAMS, Atmos. Chem. Phys., 21, 5605–5613, https://doi.org/10.5194/acp-21-5605-2021, 2021.

Pöschl, U.: Atmospheric aerosols: composition, transformation, climate and health effects, Angew. Chem. Int. Ed. Engl., 44, 7520–7540, https://doi.org/10.1002/anie.200501122, 2005.

Pratt, K. A. and Prather, K. A.: Mass spectrometry of atmospheric aerosols–recent developments and applications. Part II: On-line mass spectrometry techniques, Mass Spectrom. Rev., 31, 17–48, https://doi.org/10.1002/mas.20330, 2012.

Pratt, K. A., Mayer, J. E., Holecek, J. C., Moffet, R. C., Sanchez, R. O., Rebotier, T. P., Furutani, H., Gonin, M., Fuhrer, K., Su, Y., Guazzotti, S., and Prather, K. A.: Development and characterization of an aircraft aerosol time-of-flight mass spectrometer, Anal. Chem., 81, 1792–1800, https://doi.org/10.1021/ac801942r, 2009.

Reinard, M. S. and Johnston, M. V.: Ion formation mechanism in laser desorption ionization of individual nanoparticles, J. Am. Soc. Mass Spectrom., 19, 389–399, https://doi.org/10.1016/j.jasms.2007.11.017, 2008.

Schmidt, S., Schneider, J., Klimach, T., Mertes, S., Schenk, L. P., Kupiszewski, P., Curtius, J., and Borrmann, S.: Online single particle analysis of ice particle residuals from mountain-top mixed-phase clouds using laboratory derived particle type assignment, Atmos. Chem. Phys., 17, 575–594, https://doi.org/10.5194/acp-17-575-2017, 2017.

Silva, P. J. and Prather, K. A.: Interpretation of mass spectra from organic compounds in aerosol time-of-flight mass spectrometry, Anal. Chem., 72, 3553–3562, https://doi.org/10.1021/ac9910132, 2000.

Snyder, D. C., Schauer, J. J., Gross, D. S., and Turner, J. R.: Estimating the contribution of point sources to atmospheric metals using single-particle mass spectrometry, Atmos. Environ., 43, 4033–4042, https://doi.org/10.1016/j.atmosenv.2009.05.011, 2009.

Souto-Oliveira, C. E., Babinski, M., Araujo, D. F., and Andrade, M. F.: Multi-isotopic fingerprints (Pb, Zn, Cu) applied for urban aerosol source apportionment and discrimination, Sci. Total Environ., 626, 1350–1366, https://doi.org/10.1016/j.scitotenv.2018.01.192, 2018.

Steele, P. T., Srivastava, A., Pitesky, M. E., Fergenson, D. P., Tobias, H. J., Gard, E. E., and Frank, M.: Desorption/ionization fluence thresholds and improved mass spectral consistency measured using a flattop laser profile in the bioaerosol mass spectrometry of single Bacillus endospores, Anal. Chem., 77, 7448–7454, https://doi.org/10.1021/ac051329b, 2005.

Su, B., Zhang, G., Zhuo, Z., Xie, Q., Du, X., Fu, Y., Wu, S., Huang, F., Bi, X., Li, X., Li, L., and Zhou, Z.: Different characteristics of individual particles from light-duty diesel vehicle at the launching and idling state by AAC-SPAMS, J. Hazard. Mater., 418, 126304, https://doi.org/10.1016/j.jhazmat.2021.126304, 2021a.

Su, B., Zhuo, Z., Fu, Y., Sun, W., Chen, Y., Du, X., Yang, Y., Wu, S., Xie, Q., Huang, F., Chen, D., Li, L., Zhang, G., Bi, X., and Zhou, Z.: Individual particle investigation on the chloride depletion of inland transported sea spray aerosols during East Asian summer monsoon, Sci. Total Environ., 765, 144290, https://doi.org/10.1016/j.scitotenv.2020.144290, 2021b.

Su, Y., Wei, G., Wang, W., Xi, R., Wang, X., Xu, J., and Li, Z.: Analytical performance of single particle aerosol mass spectrometer for accurate sizing and isotopic analysis of individual particles, Atmos. Environ., 303, 119759, https://doi.org/10.1016/j.atmosenv.2023.119759, 2023.

Sun, Z., Duan, F., He, K., Du, J., and Zhu, L.: Sulfate-nitrate-ammonium as double salts in $PM_{2.5}$: Direct observations and implications for haze events, Sci. Total Environ., 647, 204–209, https://doi.org/10.1016/j.scitotenv.2018.07.107, 2019.

Tan, P. V., Malpica, O., Evans, G. J., Owega, S., and Fila, M. S.: Chemically-assigned classification of aerosol mass spectra, J. Am. Soc. Mass Spectrom., 13, 826–838, https://doi.org/10.1016/S1044-0305(02)00379-3, 2002.

Tavakoli, F. and Olfert, J. S.: Determination of particle mass, effective density, mass–mobility exponent, and dynamic shape factor using an aerodynamic aerosol classifier and a differential mobility analyzer in tandem, J. Aerosol Sci., 75, 35–42, https://doi.org/10.1016/j.jaerosci.2014.04.010, 2014.

Thomson, D. S., Middlebrook, A. M., and Murphy, D. M.: Thresholds for Laser-Induced Ion Formation from Aerosols in a Vacuum Using Ultraviolet and Vacuum-Ultraviolet Laser Wavelengths, Aerosol Sci. Tech., 26, 544–559, https://doi.org/10.1080/02786829708965452, 1997.

Vera, C. C., Trimborn, A., Hinz, K. P., and Spengler, B.: Initial velocity distributions of ions generated by in-flight laser desorption/ionization of individual polystyrene latex microparticles as studied by the delayed ion extraction method, Rapid Commun. Mass Spectrom., 19, 133–146, https://doi.org/10.1002/rcm.1753, 2005.

Wang, X. and McMurry, P. H.: A Design Tool for Aerodynamic Lens Systems, Aerosol Sci. Tech., 40, 320–334, https://doi.org/10.1080/02786820600615063, 2006.

Wang, X., Kruis, F. E., and McMurry, P. H.: Aerodynamic Focusing of Nanoparticles: I. Guidelines for Designing Aerodynamic Lenses for Nanoparticles, Aerosol Sci. Tech., 39, 611–623, https://doi.org/10.1080/02786820500181901, 2005.

Wenzel, R. J. and Prather, K. A.: Improvements in ion signal reproducibility obtained using a homogeneous laser beam for on-line laser desorption/ionization of single particles, Rapid Commun. Mass Spectrom., 18, 1525–1533, https://doi.org/10.1002/rcm.1509, 2004.

Zawadowicz, M. A., Abdelmonem, A., Mohr, C., Saathoff, H., Froyd, K. D., Murphy, D. M., Leisner, T., and Cziczo, D. J.: Single-Particle Time-of-Flight Mass Spectrometry Utilizing a Femtosecond Desorption and Ionization Laser, Anal. Chem., 87, 12221–12229, https://doi.org/10.1021/acs.analchem.5b03158, 2015.

Zawadowicz, M. A., Lance, S., Jayne, J. T., Croteau, P., Worsnop, D. R., Mahrt, F., Leisner, T., and Cziczo, D. J.: Quantifying and improving the optical performance of the

laser ablation aerosol particle time of flight mass spectrometer (LAAPToF) instrument, Aerosol Sci. Tech., 54, 761–771, https://doi.org/10.1080/02786826.2020.1724867, 2020.

Zelenyuk, A., Cai, Y., and Imre, D.: From Agglomerates of Spheres to Irregularly Shaped Particles: Determination of Dynamic Shape Factors from Measurements of Mobility and Vacuum Aerodynamic Diameters, Aerosol Sci. Tech., 40, 197–217, https://doi.org/10.1080/02786820500529406, 2006.

Zelenyuk, A., Yang, J., Song, C., Zaveri, R. A., and Imre, D.: "Depth-profiling" and quantitative characterization of the size, composition, shape, density, and morphology of fine particles with SPLAT, a single-particle mass spectrometer, J. Phys. Chem. A, 112, 669–677, https://doi.org/10.1021/jp077308y, 2008.

Zelenyuk, A., Yang, J., Choi, E., and Imre, D.: SPLAT II: An Aircraft Compatible, Ultra-Sensitive, High Precision Instrument for In-Situ Characterization of the Size and Composition of Fine and Ultrafine Particles, Aerosol Sci. Tech., 43, 411–424, https://doi.org/10.1080/02786820802709243, 2009.

Zelenyuk, A., Imre, D., Wilson, J., Zhang, Z., Wang, J., and Mueller, K.: Airborne single particle mass spectrometers (SPLAT II & miniSPLAT) and new software for data visualization and analysis in a geo-spatial context, J. Am. Soc. Mass Spectrom., 26, 257–270, https://doi.org/10.1007/s13361-014-1043-4, 2015.

Zhang, G., Han, B., Bi, X., Dai, S., Huang, W., Chen, D., Wang, X., Sheng, G., Fu, J., and Zhou, Z.: Characteristics of individual particles in the atmosphere of Guangzhou by single particle mass spectrometry, Atmos. Res., 153, 286–295, https://doi.org/10.1016/j.atmosres.2014.08.016, 2015.

Zhang, Y., Wang, X., Chen, H., Yang, X., Chen, J., and Allen, J. O.: Source apportionment of lead-containing aerosol particles in Shanghai using single particle mass spectrometry, Chemosphere, 74, 501–507, https://doi.org/10.1016/j.chemosphere.2008.10.004, 2009.

Zhou, Y., Zhang, Y., Griffith, S. M., Wu, G., Li, L., Zhao, Y., Li, M., Zhou, Z., and Yu, J. Z.: Field Evidence of Fe-Mediated Photochemical Degradation of Oxalate and Subsequent Sulfate Formation Observed by Single Particle Mass Spectrometry, Environ. Sci. Technol., 54, 6562–6574, https://doi.org/10.1021/acs.est.0c00443, 2020.

Zhu, S., Li, L., Wang, S., Li, M., Liu, Y., Lu, X., Chen, H., Wang, L., Chen, J., Zhou, Z., Yang, X., and Wang, X.: Development of an automatic linear calibration method for high-resolution single-particle mass spectrometry: improved chemical species identification for atmospheric aerosols, Atmos. Meas. Tech., 13, 4111–4121, https://doi.org/10.5194/amt-13-4111-2020, 2020.

Zhuo, Z., Su, B., Xie, Q., Li, L., Huang, Z., Zhou, Z., Mai, Z., and Tan, G.: Improved Aerodynamic Particle Concentrator for Single Particle Aerosol Mass Spectrometry:A Simulation and Characterization Study, Chinese Journal of Vacuum Science and Technology, 41, 443–449, https://doi.org/10.13922/j.cnki.cjvst.202008026, 2021.